Hindawi
Geofluids
Volume 2022, Article ID 8351316, 17 pages
https://doi.org/10.1155/2022/8351316

Research Article

Research on Fracture Characteristics and Energy Dissipation of Hard Rock under the Excitation of Ultrasonic Vibration

Lei Zhang,[1,2] Xufeng Wang,[1,3] Jiyao Wang,[1] and Zhanbiao Yang[2]

[1]*School of Mines, China University of Mining and Technology, Jiangsu Engineering Laboratory of Mine Earthquake Monitoring and Prevention, Xuzhou 221116, China*
[2]*State Key Laboratory of Coking Coal Exploitation and Comprehensive Utilization, China Pingmei Shenma Group, Pingdingshan 467000, China*
[3]*State Key Laboratory of Coal Resources and Safe Mining, China University of Mining and Technology, Xuzhou 221116, China*

Correspondence should be addressed to Xufeng Wang; wangxufeng@cumt.edu.cn

Received 8 September 2022; Revised 8 December 2022; Accepted 12 December 2022; Published 23 December 2022

Academic Editor: Tianshou Ma

To promote the application of ultrasonic vibration rock crushing technology in underground rock-drilling engineering, it is necessary to investigate the damage and fracture characteristics of hard rock under the excitation of ultrasonic vibration. In this study, the brittle red sandstone was taken as the research object, the rock fracture experiments under the excitation of ultrasonic vibration were carried out, and the macrodeformation of rock samples was monitored by strain gauges. The experimental results show that the strain curve of rock samples under the excitation of ultrasonic vibration can be divided into the compaction stage, elastic deformation stage, and damage stage; with the increase in static load, the maximum intrusion depth and maximum failure depth of rock samples increase exponentially. To study the damage evolution and energy dissipation mechanism of rock samples under the excitation of ultrasonic vibration, a numerical model was established by using particle flow software PFC2D. The results show that the proposed model can effectively simulate the failure characteristics of rock samples under the excitation of ultrasonic vibration. Through the analysis of the displacement field, stress field, and dynamic fracture process of rock samples, the damage and fracture mechanism of rock samples under the excitation of ultrasonic vibration were revealed. In addition, the ultrasonic vibration simulation tests on rock samples were carried out under different static loads, and the number of rock cracks and energy dissipation process were monitored in real time. The results show that static loads can accelerate the initiation and propagation of cracks and improve the utilization rate of rock crushing energy.

1. Introduction

In underground mining, rock mass with high hardness is widely distributed in the strata, which greatly affects the mining efficiency. Traditional rock crushing methods have the disadvantages of large energy consumption and high cost. Therefore, an efficient and low-consumption method for hard rock crushing is urgently needed. As a new rock crushing technology, ultrasonic vibration rock crushing technology has been first applied to the field of space sampling and polar exploration, and its research focuses on the development of ultrasonic samplers [1, 2]. Wiercigroch et al. [3] developed a set of ultrasonic vibration rock crushing test devices and established the corresponding dynamic model. In this test, experimental research and theoretical analysis were firstly combined, and the results show that the failure speed of the rock sample under high-frequency axial vibration impact is significantly improved. Zhao and Sangesland [4] conducted a mechanical analysis of the rock crushing process of ultrasonic vibration cutting. It was found that the contact force between rock and drilling tool under the ultrasonic vibration greatly reduces the wear of drill bit. Therefore, compared with traditional rock crushing methods, ultrasonic vibration rock crushing technology can better meet the needs of efficient rock crushing in underground engineering and has a high application prospect.

In the ultrasonic vibration rock crushing technology, the high-frequency cyclic load is applied to the rock mass by drilling tools to induce the rapid fatigue damage of the rock and realize the efficient fracture of the rock mass. Research on the damage and failure characteristics of rock mass under cyclic loading has been widely conducted. Li et al. [5] established a fatigue damage model of the jointed rock mass under cyclic compression load. Based on test data, it was found that the deformation modulus of the rock mass increased with the increase of impact frequency. Bagde and Petros [6] studied the influence of cyclic load parameters on dynamic mechanical parameters of the rock mass through experiments. The results showed that the dynamic axial stiffness and fatigue strength of the rock sample were positively correlated with cyclic load amplitude and frequency. Yang et al. [7] analyzed the influence of crack parameters on mechanical behaviors of rock samples. It was found that the change of crack density, inclination, and spacing could affect the strength and failure mode of rock samples. By using fractal theory, Li et al. [8] explored the law of rock fragmentation under cyclic loading and found that the greater the cyclic loading rate, the higher the degree of rock fragmentation and the more uniform the fragmentation. Liu and He [9] investigated the influence of confining pressure on the mechanical properties of rock samples under cyclic loading and analyzed the fatigue damage of sandstone under the confining pressure by the residual strain method. It was concluded that the shear fracture surface of rock could be widened by the increase of confining pressure.

In the above studies, the cyclic load frequency is lower than 100 Hz, while the previous research [10] has shown that the mechanical response of rock varies with the change of load frequency. At present, some researchers have summarized the response and failure characteristics of rock mass under high-frequency vibration. Through the finite element method, Li et al. [11] analyzed the resonance characteristics of rock samples under harmonic excitation. The results showed that the resonance frequency of rock samples was affected by rock size and mechanical parameters. Based on the self-developed ultrasonic vibration excitation device, Yin et al. [12] analyzed the influence of static load on the mechanical strength of granite samples and obtained an optimal static load to maximize the damage degree of the rock sample. Zhou et al. [13] investigated the deformation characteristics of granite during ultrasonic vibration excitation through strain experiments and divided the deformation process of rock into three stages, elastic deformation, plastic deformation, and damage stages. By using a scanning electron microscope (SEM), Zhao et al. [14] observed the microcrack propagation characteristics of granite under ultrasonic vibration and concluded that the internal feldspar particles has the largest effect on the damage of granite samples. It was found that the failure time of granite and the maximum crack propagation length were the smallest. Zhang et al. [15] obtained the evolution law of rock pores under the ultrasonic vibration through the nuclear magnetic resonance (NMR) test. The results showed that high-frequency vibration could better promote the development of rock pores.

Figure 1: Red sandstone specimens.

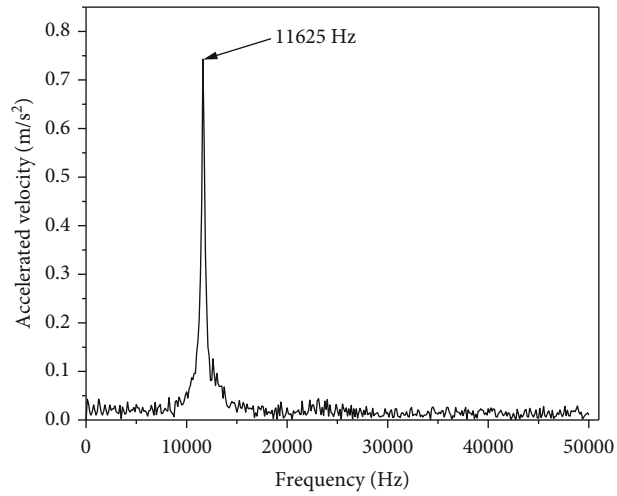

Figure 2: Natural frequencies of red sandstone.

However, the above experimental studies mostly use granite samples as hard rocks and rarely analyze the crushing law of rock samples under high-frequency vibration from the perspective of energy. In this study, the brittle red sandstone was taken as the research object. The ultrasonic vibration rock crushing test was carried out to obtain the progressive fracture characteristics of rock samples under different static loads, and the influence of static loads on the fracture range was studied. Besides, the ultrasonic vibration excitation experiments on rock samples were simulated by the particle flow software PFC2D, and the microcrack evolution and energy dissipation law of rock samples were explored in this process.

2. Rock Crushing Experiment under the Excitation of Ultrasonic Vibration

2.1. Specimen Preparation. The red sandstone used in the experiment was a common hard brittle rock taken from Sichuan Province, China. Firstly, the rock block was processed into a standard cylinder sample with a diameter of 50 mm and a height of 100 mm, as shown in Figure 1. Both the size, flatness, parallelism, and perpendicularity of the rock sample were in accordance with International Society for Rock Mechanics (ISRM) standard [16]. Secondly, the physical parameters of rock samples were calculated. The average density of the red sandstone sample in a natural

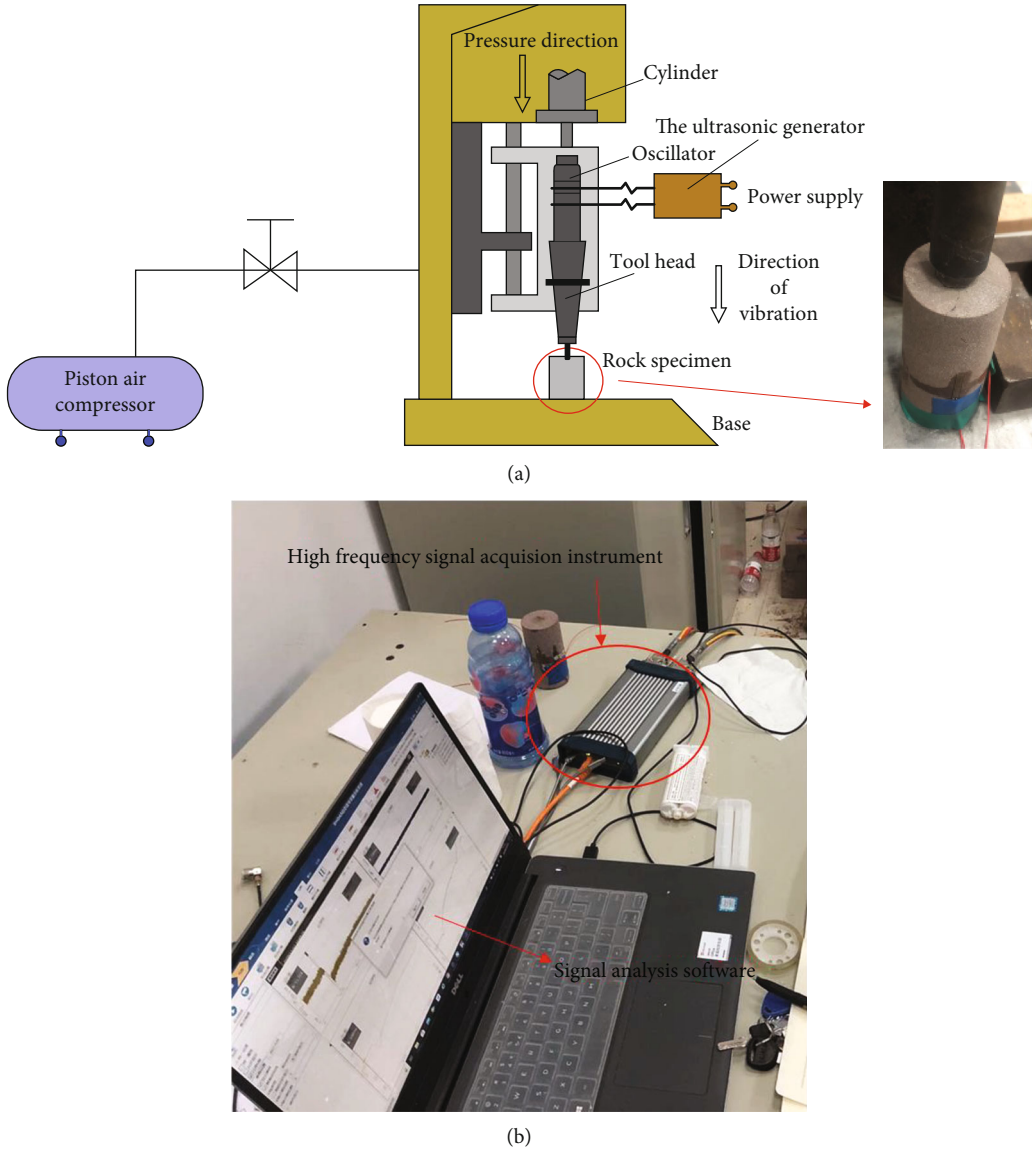

Figure 3: (a) Rock breaking device excited by ultrasonic vibration. (b) Strain monitoring system.

state was 2.7 g/cm^3, and the average longitudinal wave velocity was 4110 m/s. Thirdly, the basic mechanical parameters of rock samples were obtained through the uniaxial compression test. The average uniaxial compressive strength and elastic modulus were 92.5 MPa and 5.4 GPa. The average porosity of rock obtained by NMR technology was 7.5%. To reduce the influence of the difference in natural frequency on the experimental results, the natural frequency of rock samples was measured by the knocking method [17], and the sample with the natural frequency of 11650 ± 50 Hz was selected. Figure 2 shows the natural frequency test results of a rock sample.

2.2. Test System. The test system includes two parts, an ultrasonic high-frequency vibration excitation device and a signal acquisition system. Figure 3 shows the ultrasonic high-frequency vibration excitation device. The vibration loading device mainly includes the ultrasonic generator, oscillator, tool head, and piston air compressor. The oscillator converts electrical signals into mechanical vibration signals, the ultrasonic amplitude transformer amplifies the vibration amplitude and acts on the rock through the tool head connected with it, and the air compressor is used to apply adjustable static load to the rock sample. The signal acquisition system includes the high-frequency signal acquisition instrument, signal analysis software, and strain gauge, and this system is used to monitor the axial strain of rock samples during excitation.

2.3. Test Process. In this test, three groups of ultrasonic vibration excitation tests were designed, the vibration frequency and amplitude were 20 kHz and 70 μm, and the static loads of each group were set to be 0.15 MPa, 0.2 MPa, and 0.25 MPa, respectively. The excessive excitation time can cause the rise of rock temperature, which affects the test results of strain. To avoid this condition, the interval

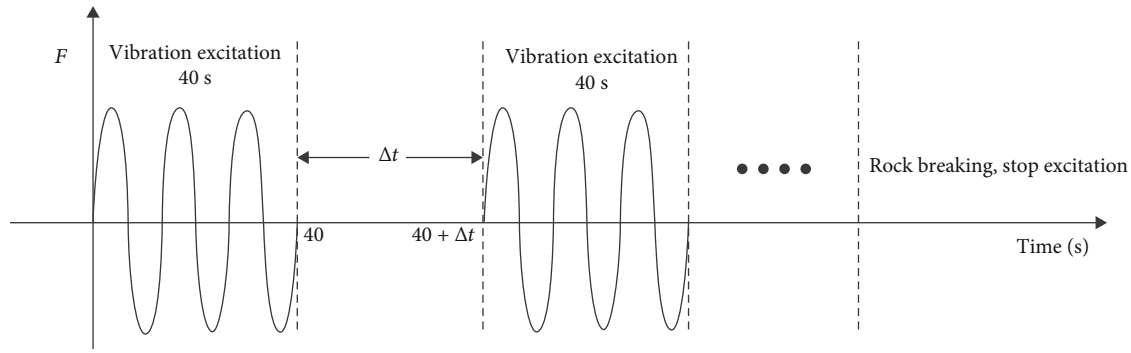

Figure 4: Interval vibration excitation mode.

vibration excitation method was adopted in this test, as shown in Figure 4. The strain data was recorded and the rock samples were observed every 40 s after excitation. After a period of time, the next excitation was carried out until rock failure occurred, and the cumulative time of rock sample failure was recorded.

3. Analysis of Test Results

3.1. Dynamic Damage Process of Rock Samples. The macrodeformation of rock mass reflects the damage law of the rock sample. The initiation and propagation of crack can increase the macrodeformation [18]. When the rock is broken, the failure of the strain gauge occurs and the strain value gradually returns to 0. The experiment shows that the fracture of rock sample occurs within 40 s under a static load of 0.25 MPa. Figure 5 shows the strain-time curve of the rock sample during this process. The deformation process of rock samples can be divided into three stages, compaction stage, elastic deformation stage, and damage stage.

(1) Compaction stage: at this stage, natural cracks exist in the rock and are rapidly compacted under the action of ultrasonic vibration load, and the strain value of the rock sample increases linearly

(2) Elastic deformation stage: as shown in Figure 5, after 3.4 s vibration excitation, the strain curve tends to be flat, and the slope of the curve is close to 0. At this time, the rock is equivalent to an elastic body, and slight elastic deformation occurs under the influence of vibration load

(3) Damage stage: after 7.1 s vibration excitation, new microcracks are continuously generated in the rock sample. Under the influence of compaction in the axial direction, the deformation amount begins to grow nonlinearly, and the cracks are developed and gradually penetrated to form macrocracks. Finally, the rock fracture occurs at 13.3 s

3.2. Progressive Process of Rock Failure. By recording the rock failure after each vibration excitation, the progressive law of rock failure is obtained. It is found that the fracture law of the rock sample under different static loads is similar. Figure 6 shows the typical failure process of the rock sample under a static load of 0.15 MPa. The rock in the contact area between the rock and the tool head is constantly broken into powder, and a circular fracture zone is first formed on the

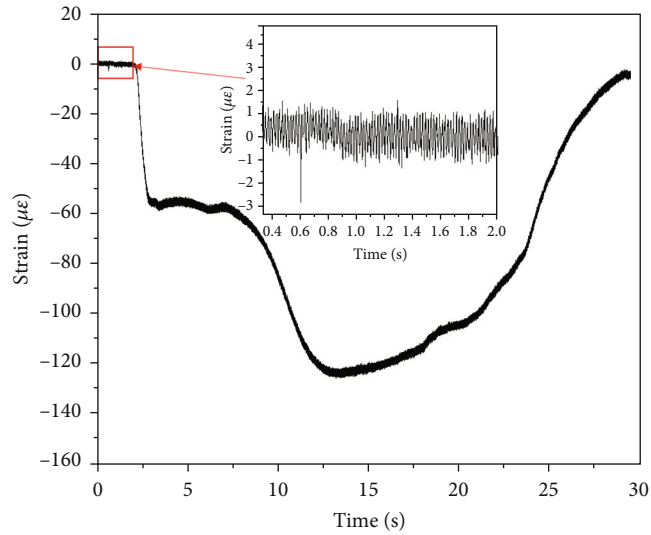

Figure 5: Axial strain of rock.

excitation surface. With the progress of the vibration excitation, the area and depth of the fracture zone increase. At the same time, macrocracks are constantly generated from the edge of the area and spread in the radial and axial directions. When two adjacent macrocracks are connected, the broken block is generated and detached from the rock sample. It can be seen that local failure of the rock sample occurs under the excitation of ultrasonic vibration, and the closer the rock is to the excitation surface, the greater the damage. Besides, there is a maximum intrusion depth of the rock sample. After reaching the maximum intrusion depth, the macrocracks are quickly penetrated, and then rock failure can be caused.

To further study the influence of static load on rock fracture, the failure modes of rock samples under different static loads are compared, as shown in Figure 7. It can be found that the greater the static load, the shorter the time required for rock failure. Compared with that under the static load of 0.15 MPa, the time required for rock failure at the static load of 0.2 MPa and 0.25 MPa is shortened by 73.48% and 85.43%, respectively. The increase of static load also increases the maximum intrusion depth of the rock sample, and the longitudinal propagation of macrocracks is deeper,

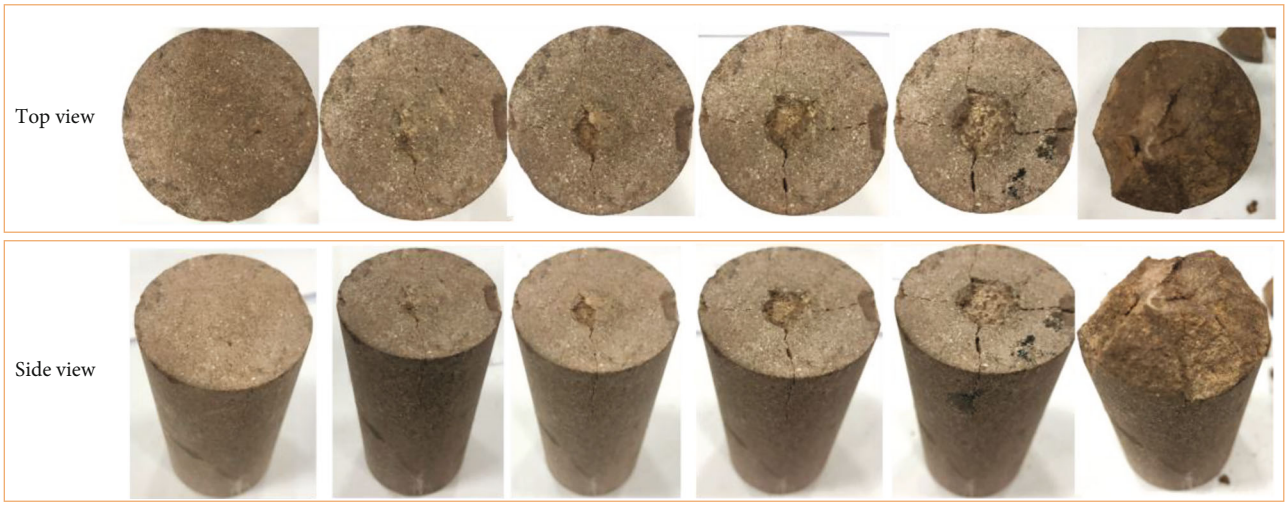

Figure 6: Progressive process of rock failure.

resulting in larger fragments during failure. Figure 7(b) shows the variation curve of the maximum intrusion depth and the maximum crack propagation depth with the static load. With the increase of static load, the final failure range of the rock sample increases exponentially.

The process of rock deformation and failure is accompanied by energy conversion and microcrack evolution. Therefore, the law of energy dissipation and crack evolution in the rock sample under the excitation of ultrasonic vibration can be analyzed from a mesoscopic perspective, which is conducive to illustrating the internal mechanism of rock failure under high-frequency vibration.

4. Particle Flow Simulation of Ultrasonic Vibration Excitation Test

4.1. Establishment of Particle Flow Numerical Model. Based on the discrete element analysis, the PFC2D software can be used to study the damage and fracture mechanism of rock-like materials from the perspective of mesomechanics. The model in PFC2D software is composed of particles, walls, contacts, bonds, and other units. The rock-like materials are constructed as a collection of particles of various sizes, and the adjacent two particles are connected by the contact model. When the particle flow program is used, the constitutive relationship and material characteristics of the material model do not need to be defined, but the macro- and mesomechanical parameters of the material need to be combined. The parallel bond model was proposed by Potyondy [19], and the existing studies [20, 21] have proven that this model can accurately simulate the microcrack propagation of rock materials. Therefore, the parallel bond model is used to simulate the brittle red sandstone in this study.

In the parallel bond model, both force and torque can be transmitted. Figure 8 shows the parallel bond model. The parallel bond contact is added between adjacent particles, and the contact range is a square area. In the PFC2D method, the stress on the parallel bond model can be calculated as follows:

$$\sigma = \frac{-\overline{F}_i^n}{A}, \tag{1}$$

$$\tau = \frac{\left|\overline{F}_i^s\right|}{A}, \tag{2}$$

where σ and τ represent the normal force and tangential force applied to the bonding key, and A represents the area of the parallel bond area.

The mesomechanical parameters of the model directly determine its macromechanical behavior, and the macromechanical parameters can be obtained by the uniaxial compression test. A red sandstone sample with a diameter of 50 mm and a height of 100 mm is established by the parallel bond model, and the particle flow program [22] is compiled to determine the mesoparameters of the model. The model includes 6,965 particles, with a maximum particle radius of 0.35 mm and a minimum particle radius of 0.25 mm. Table 1 shows the specific mesomechanical parameters. Figure 9 shows the comparison between uniaxial compression simulation results and test results. It can be seen that the rock model with these mesomechanical parameters can accurately reflect the mechanical characteristics of red sandstone. Therefore, this model can be used to simulate rock fracture under the excitation of ultrasonic vibration.

When using PFC2D to simulate ultrasonic vibration rock crushing, the vibration excitation load can be simulated by adding velocity boundary [23]. According to the application principle of ultrasonic vibration load, the displacement boundary of vibration load can be expressed as follows:

$$x = A \cdot \sin\left(2\pi f \cdot t\right), \tag{3}$$

where x is the displacement of the excitation surface; A is the amplitude; f is the ultrasonic vibration frequency; t is the excitation time. By differentiating the displacement of the

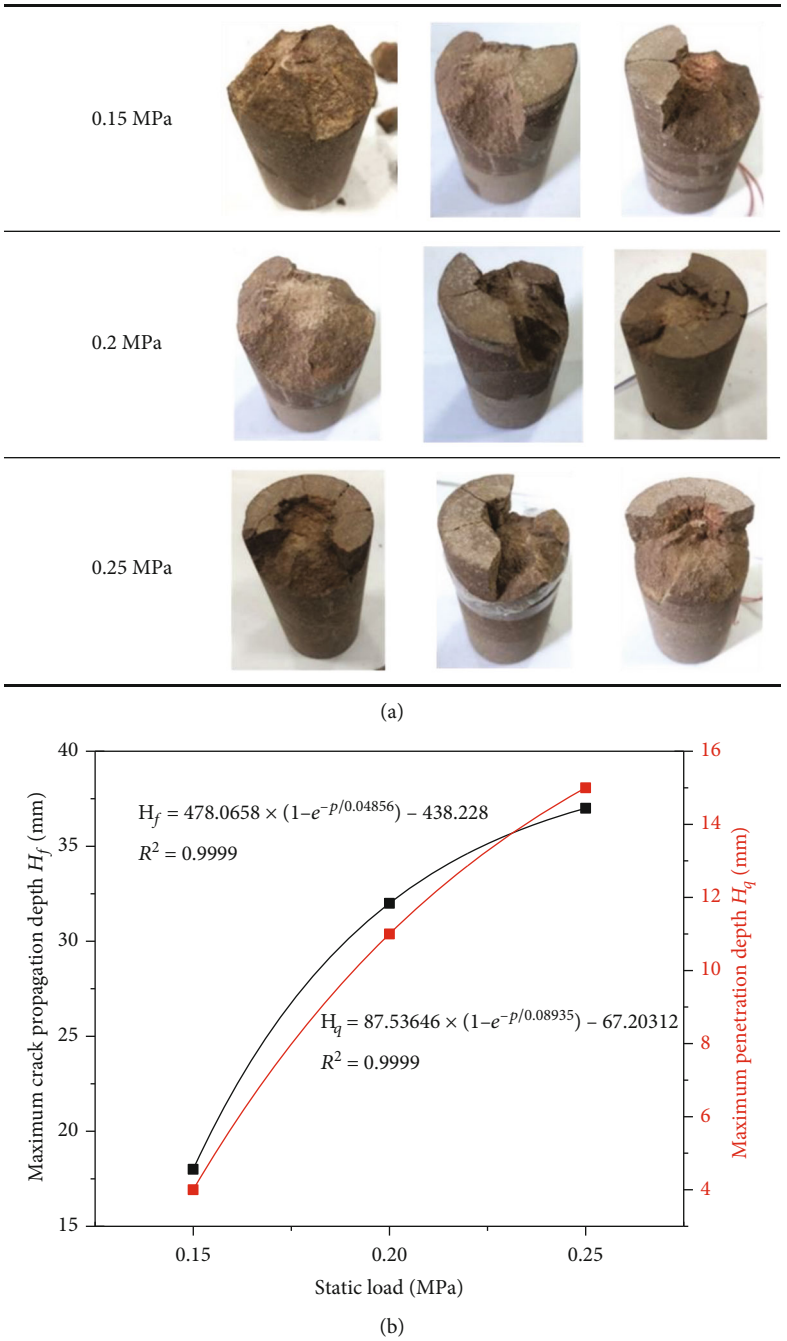

Figure 7: Failure characteristics of rock under different static loads. (a) Rock failure mode. (b) Relationship between static load and maximum penetration depth and maximum destruction depth.

excitation surface, the velocity boundary can be obtained as follows:

$$v = A \cdot 2\pi f \cdot \cos(2\pi f \cdot t). \tag{4}$$

4.2. Energy Theory in PFC2D. The process of rock deformation and failure is accompanied by energy conversion, and energy dissipation reflects the development characteristics of internal damage of the rock sample. When PFC2D is used for numerical simulation, the changes of various energies during the test can be tracked in real time [24], which can facilitate the understanding of the simulation results. It is assumed that there is no heat exchange between the rock mass and the outside world in the process of rock deformation and failure. According to the law of energy conservation, the total work exerted by the external load on the rock can be described as follows: [25]

$$W_b = W_e + W_d, \tag{5}$$

where W_e is the total elastic strain energy and W_d is the dissipation energy. In the simulation, the following energies are

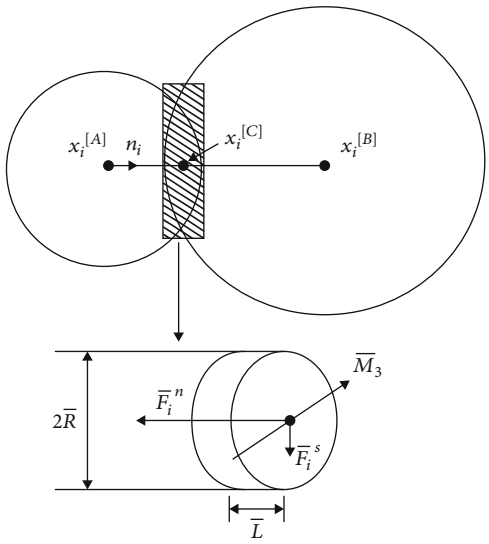

Figure 8: Parallel bond model.

involved: parallel bond strain energy (W_{pb}), particle strain energy (W_c), friction energy (W_f), plastic deformation energy (W_β), and kinetic energy (W_k). Among them, the parallel bond strain energy (W_{pb}) is the strain energy generated by all the parallel bonds in the model; the particle strain energy (W_c) refers to the sum of the strain energy stored in the contact spring; the friction energy (W_f) refers to the energy consumed by the staggered friction of the particles in the model; the plastic deformation energy (W_β) refers to the energy consumed by the plastic deformation, and the kinetic energy (W_k) refers to the energy generated by the particle movement, including rotation and translation of the particles. The total strain energy can be calculated as follows: [26]

$$\begin{cases} W_e = W_{\mathrm{pb}} + W_c, \\ W_{\mathrm{pb}} = \dfrac{1}{2}\displaystyle\sum_{N_{\mathrm{pb}}}\left(\frac{\left|\overline{F}_i^{\,n}\right|^2}{\left(A\overline{k}_n\right)} + \frac{\left|\overline{F}_i^{\,s}\right|^2}{\left(A\overline{k}_s\right) + \overline{M}_3{}^2/I\overline{k}_n}\right), \\ W_c = \dfrac{1}{2}\displaystyle\sum_{N_c}\left(\frac{\left|\overline{F}_i^{\,n}\right|^2}{\overline{k}_n} + \frac{\left|\overline{F}_i^{\,s}\right|^2}{\overline{k}_s}\right). \end{cases} \tag{6}$$

The dissipation energy and kinetic energy can be calculated by the following equations: [27]

$$\begin{cases} W_d = W_f + W_\beta, \\ W_f \longleftarrow W_f - \displaystyle\sum_{N_c}\left(F_i^{\,s}\left(\Delta U_i^{\,s}\right)^{\mathrm{slip}}\right), \end{cases} \tag{7}$$

$$W_k = \frac{1}{2}\sum_{N_p}\sum_{i=1}\varsigma_{(i)}\upsilon^2{}_{(i)}, \tag{8}$$

where N_{pb} represents the number of parallel bond keys; $\bar{F}_i^{\,n}$ represents the normal stress of parallel bond; $\bar{F}_i^{\,s}$ represents the tangential stress of parallel bond; k_n and k_s are the normal stiffness and tangential stiffness; I and A are the inertia moment and cross-sectional area of the parallel bond; $\bar{M}_3$ is the torque; N_c is the number of contacts; N_p is the number of particles; $F_i^{\,s}$ is the tangential contact force; $\varsigma_{(i)}$ and $\upsilon_{(i)}$ represent particle mass and velocity, respectively; $(\Delta U_i^{\,s})^{\mathrm{slip}}$ represents the slip amount, and it can be calculated as follows:

$$\left(\Delta U_i^{\,s}\right)^{\mathrm{slip}} = \frac{\left(\Delta U_i^{\,s} + \left(\left(F_i^{\,s}\right)^{(t+\Delta t)} - \left(F_i^{\,s}\right)^t\right)\right)}{\overline{k}_s}. \tag{9}$$

According to Equation (5), the dissipation energy can be deduced and expressed below:

$$W_d = W_b - W_e - W_k. \tag{10}$$

The calculation equation of total energy W_b is

$$W_b = \sum_{N_w}\left(F_i \Delta U_i + \overline{M_3}\Delta\theta_3\right), \tag{11}$$

where F_i is contact force, $\triangle U_i$ is the particle displacement, $\Delta\theta_3$ is the particle angle, and N_w is the number of walls.

5. Simulation Results and Analysis

The simulation results and experimental results of rock failure under the excitation of ultrasonic vibration are compared, as shown in Figure 10. The failure mode of rock samples obtained from numerical simulation is highly similar to that of indoor experimental results. It indicates that the numerical model with these mesoparameters can also reflect the mechanical properties of the rock mass under high-frequency vibration excitation, which further verifies the accuracy of the proposed model.

5.1. Displacement Field and Damage Evolution. Figure 11 shows the distribution of the internal displacement field of rock samples under the excitation of ultrasonic vibration. With the increase of calculation steps, the displacement field gradually diffuses from the fan-shaped small area below the top excitation surface to the whole rock, and gradually tends to be stable. The displacement field shows an obvious layering effect and can be divided into three main layers. The first layer is the fan-shaped high-level displacement field formed under the excitation surface, while the third low-level displacement field is distributed in the bottom area, and the particle displacement in this area is little affected by the vibration load. Besides, there is a large displacement difference at the junction of the first layer and the second layer, and the particle bond at the junction of the two layers is more prone to fracture, leading to the generation of microcracks.

Figure 12 shows the crack initiation and propagation process of rock samples under the excitation of ultrasonic vibration. In this figure, shear cracks are marked in blue and tensile cracks in red. Under the excitation of ultrasonic

Table 1: Mesomechanical parameters of red sandstone.

Particle density/(kg/m^3)	Particle stiffness ratio	Parallel bond modulus (GPa)	Parallel bond stiffness ratio	Parallel bond radius factor
2700	1.5	4.5	2.5	1
Particle contact modulus	Normal bond strength	Tangential bond strength	Friction coefficient	Particle Size ratio
4.8	37	45	0.5	1

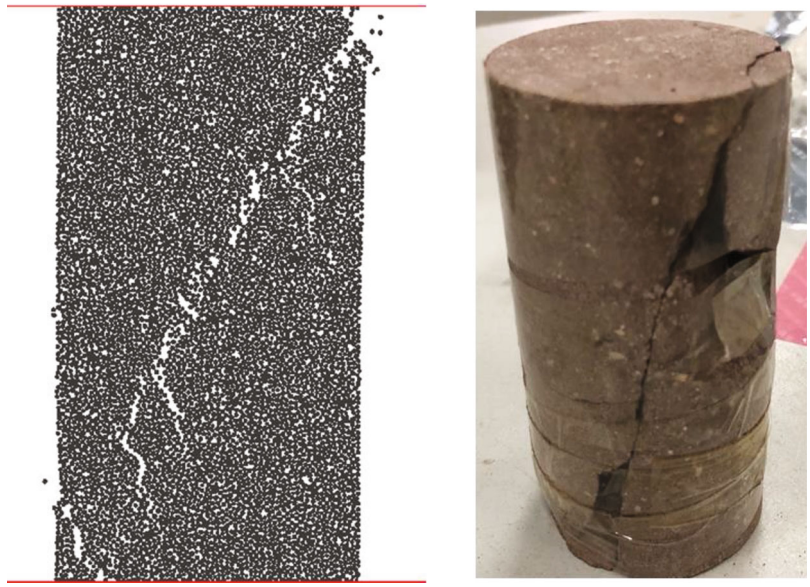

(a)

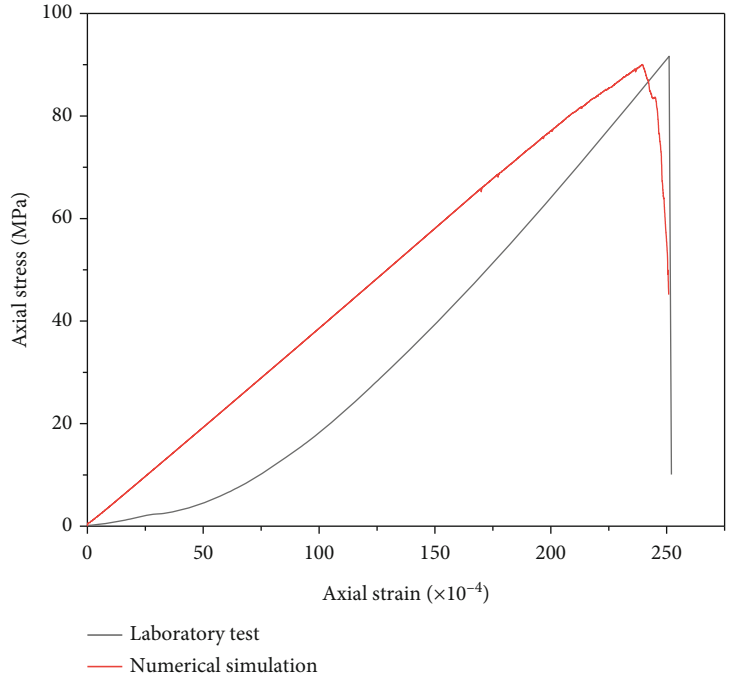

(b)

Figure 9: Comparison between simulation results and test results: (a) uniaxial failure mode (b) stress-strain curve.

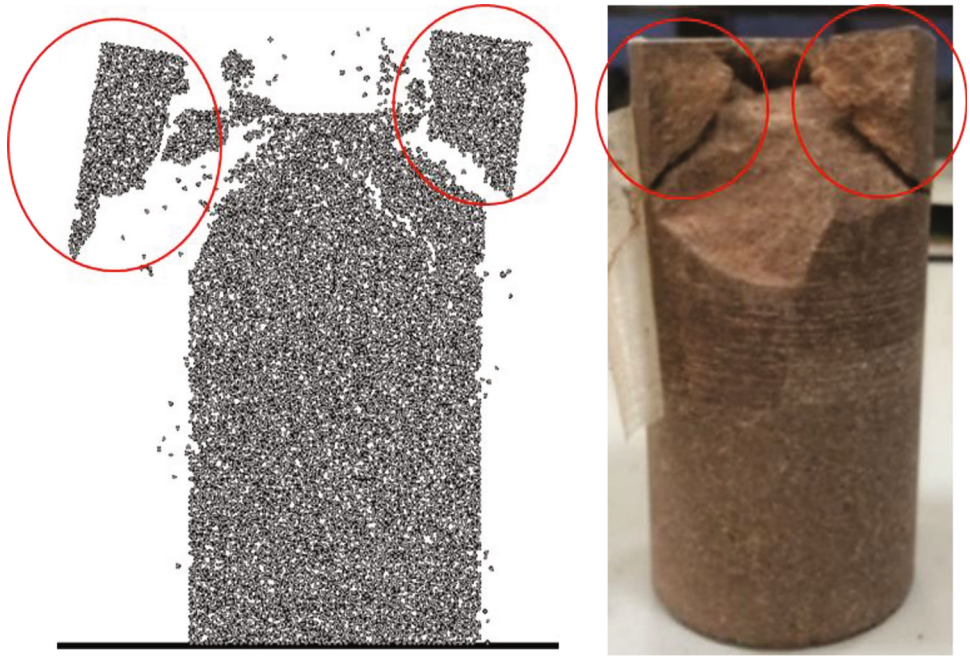

Figure 10: Comparison of failure modes between simulation and test.

vibration, the shear failure first occurs in the area of the maximum shear stress below the excitation surface of the rock sample. Under the action of stress concentration, the edge area of the excitation surface is fractured, and a group of cracks is generated and expands toward the direction of the maximum shear stress. As a result, an X-shaped macrofracture zone is gradually formed in the rock mass. When the fracture zone develops to the free surface at both ends, the broken block is formed and peels off from the rock surface. The failure mode of the rock mass is consistent with that in the laboratory experimental results.

Figure 13 shows the proportion of shear cracks and tensile cracks under the excitation of ultrasonic vibration. The tensile cracks are mainly produced in the whole process. The fracture of particle bonds in the rock is caused by the shear failure at the initial excitation stage. With the continuous development and expansion of cracks, the proportion of tensile cracks increases rapidly and tends to be stable gradually. When the rock fracture occurs, the cumulative proportion of tensile cracks reaches 74.2%. The change of acoustic emission count under the excitation of ultrasonic vibration is shown in Figure 14. The damage degree of the rock mass during vibration can be expressed by the following equation: [28]

$$n = \frac{\sum_{i=1}^{m} r_i l_i}{\sum_{i=1}^{M} r_i l_i}, \tag{12}$$

where n represents the damage coefficient; m and M represent the current calculation steps and the total number of cracks accumulated during rock fracture; r_i and l_i represent the radius and length of the i-th crack. As shown in Figure 14, the damage process of the rock mass can be divided into four stages, initial vibration excitation stage, crack initiation stage, rapid crack propagation stage, and slow crack growth stage. In the initial vibration excitation stage, no acoustic emission signal is generated. In the crack initiation stage (a, b), the number of cracks increases slowly, and the cumulative shear cracks in this stage account for 81.8%. In the rapid crack propagation stage (b, c), the number of cracks increases rapidly, and the damage curve generally shows a linear increasing trend. Besides, the proportion of tensile cracks increases from 18.2% to 73.4%, with an increase of 303.3%. When the damage coefficient increases to 0.88, the slow crack growth stage (c, d) is reached, and the damage rate of the rock mass slows down.

Since the force and velocity loads cannot be applied to wall boundary simultaneously in PFC2D software, researchers have found that the increase of static load can increase the vibration amplitude of the system [29]. Therefore, different static loads can be characterized by changing the vibration amplitude. To further study the influence of static load on the evolution of microcracks in the rock mass, four ultrasonic vibration excitation experiments (U1-U4) on rock samples were designed, and the amplitudes of ultrasonic vibration were set as 70 mm, 75 mm, 80 mm, and 85 mm, respectively. Figure 15(a) shows the evolution comparison of microcracks in rock samples under four working conditions. It can be found that the static load accelerates crack initiation and promotes crack propagation, and the cumulative number of cracks in rock increases with the increase of static load. Figure 15(b) shows the proportion curve of the number of tensile cracks under different static loads. It can be seen that the proportion of tensile cracks generated by the excitation process is less affected by static loads, and the proportion of tensile cracks is always maintained at about 75%.

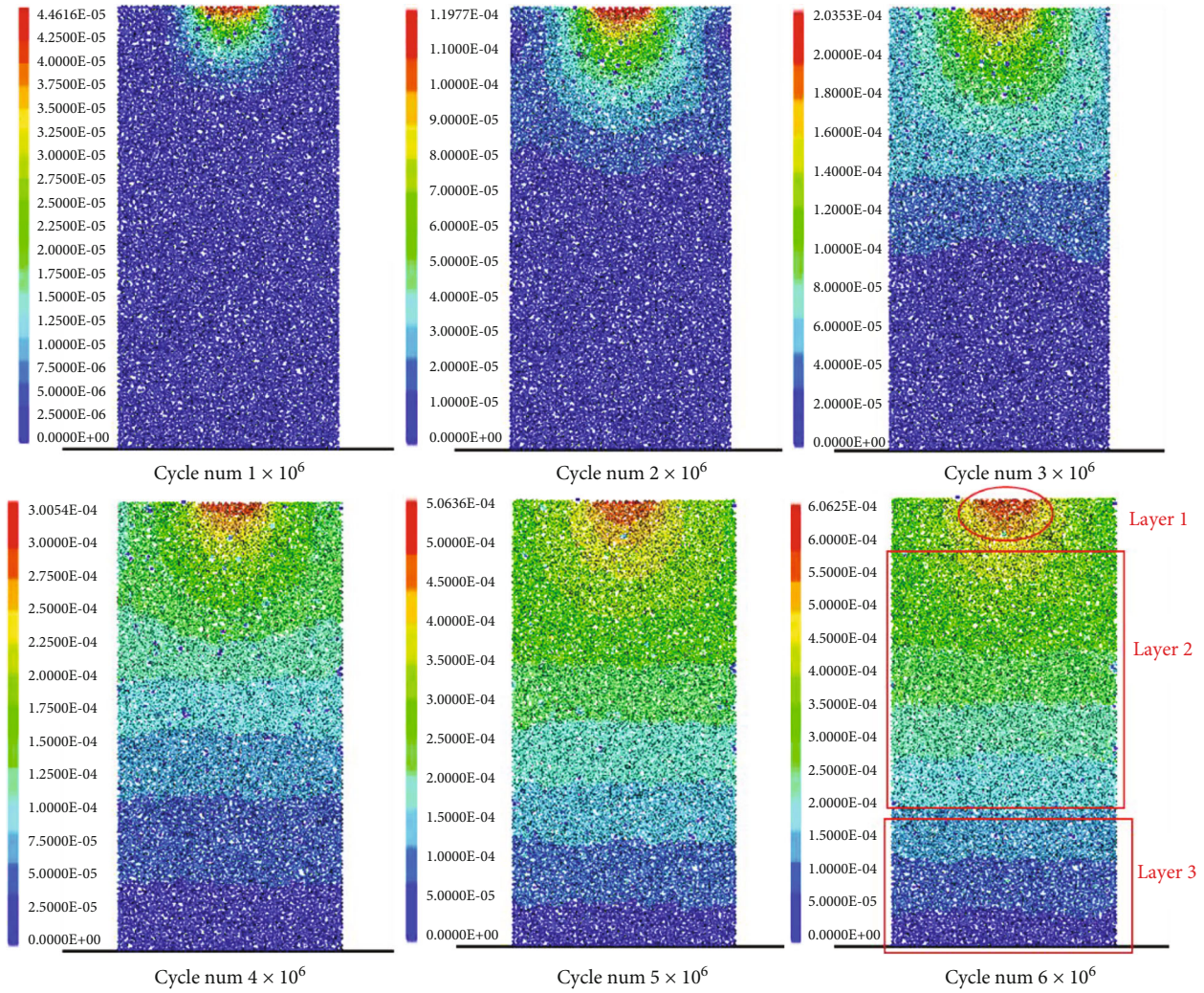

Figure 11: Distribution of displacement field in rock under ultrasonic vibration excitation.

5.2. Stress Field Distribution. Figure 16 shows the internal stress distribution of the rock sample under different cycle numbers. Under the ultrasonic vibration load, the internal stress of the rock sample increases continuously; there is always an obvious high-stress concentration area near the excitation surface, while the stress variation in the rock region far from the excitation surface is little affected by the vibration load. In addition, a small range of high-stress areas can be observed in other local areas. This is because the microcracks expand and converge to form macroscopic cracks, and stress concentration also occurs at the crack tip under the action of vibration load. Under the action of vibration load, the crack tip will also produce stress concentration. At the same time, the intersection of compressive stress and tensile stress occurs in the fracture of the rock mass.

To reflect the macroscopic mechanical properties of rocks under load, the transfer process of the contact forces between particles can be visualized to form force chains in the PFC2D model. Figure 17 shows the distribution of the contact force chain inside the rock under the excitation of ultrasonic vibration, in which compressive force is marked as black and tensile stress as red. The thicker the force chain, the stronger the contact force. After the rock is loaded by ultrasonic vibration, a strong stress chain concentration area is formed on the excitation surface, and the strong stress chain diffuses to the lower part in a fan shape. The rest of the rock mass is less affected by the vibration load, and the force chain is evenly distributed. The macrocrack propagates to the deep along the transmission path of the strong stress chain and reaches the free surface, then the failure of the rock mass is caused.

5.3. Energy Dissipation. Figure 18(a) shows the energy evolution curve under the excitation of ultrasonic vibration. Since the kinetic energy generated in the whole process is extremely small, it can be ignored in this study. At the initial stage of vibration excitation, almost all the input energy is converted into strain energy, and the strain energy increases exponentially. When the internal stress of rock increases continuously and exceeds the elastic limit, the fracture of particle bond occurs, and the mesocracks are gradually formed, leading to the continuous generation and increase of dissipated energy. More input energy is transformed into

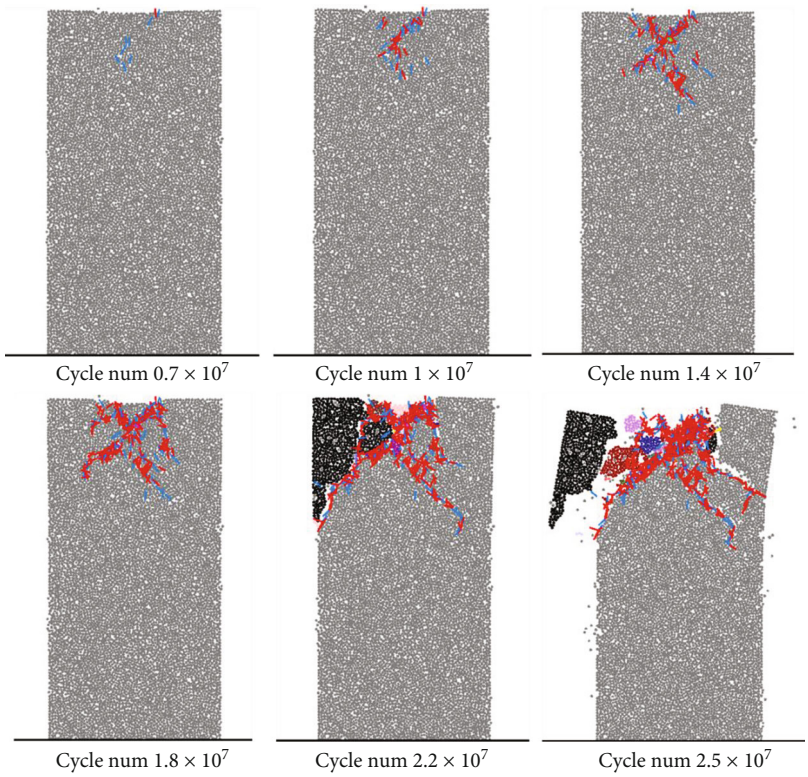

Figure 12: Crack evolution in rock under ultrasonic vibration excitation.

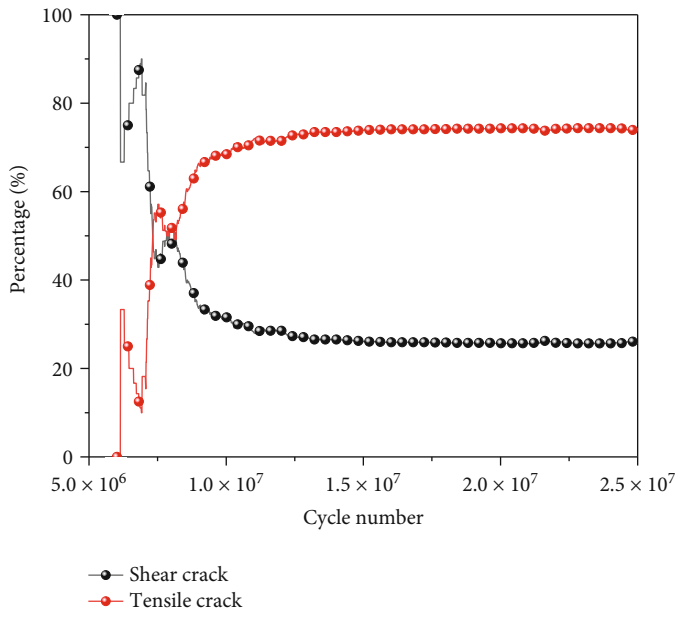

Figure 13: The proportion of shear and tensile cracks under ultrasonic vibration excitation.

friction energy and plastic deformation energy, and the increase of strain energy is gradually lower than that of input energy. When the strain energy reaches the peak value, the rock failure occurs, and the strain energy is released rapidly in the form of friction energy and plastic deformation energy, while the dissipated energy rises rapidly. The increase of plastic deformation energy indicates the continuous development of microcracks in the rock, while the increase of friction energy indicates that the more frequent staggered friction between particles causes the increase of internal energy in the rock mass.

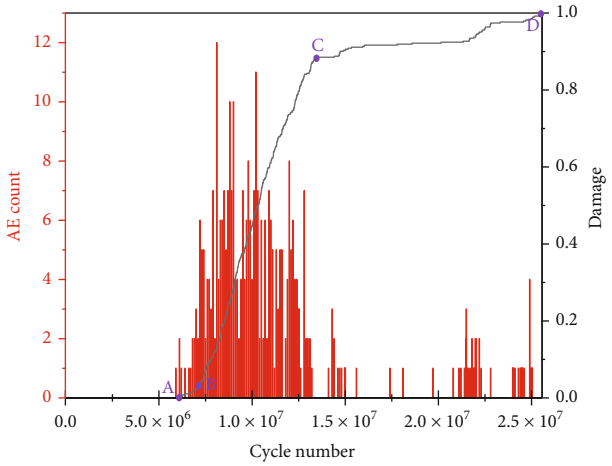

Figure 14: Acoustic emission counts.

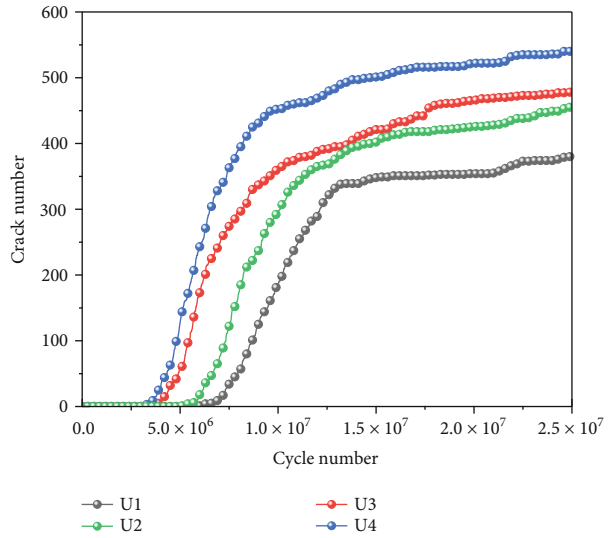

(a)

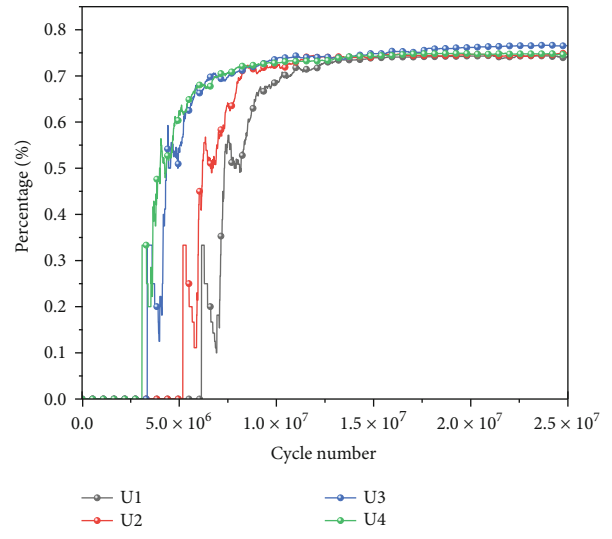

(b)

Figure 15: Variation of the number of cracks in rock under different static loads. (a) Total number of cracks. (b) Tensile crack proportion.

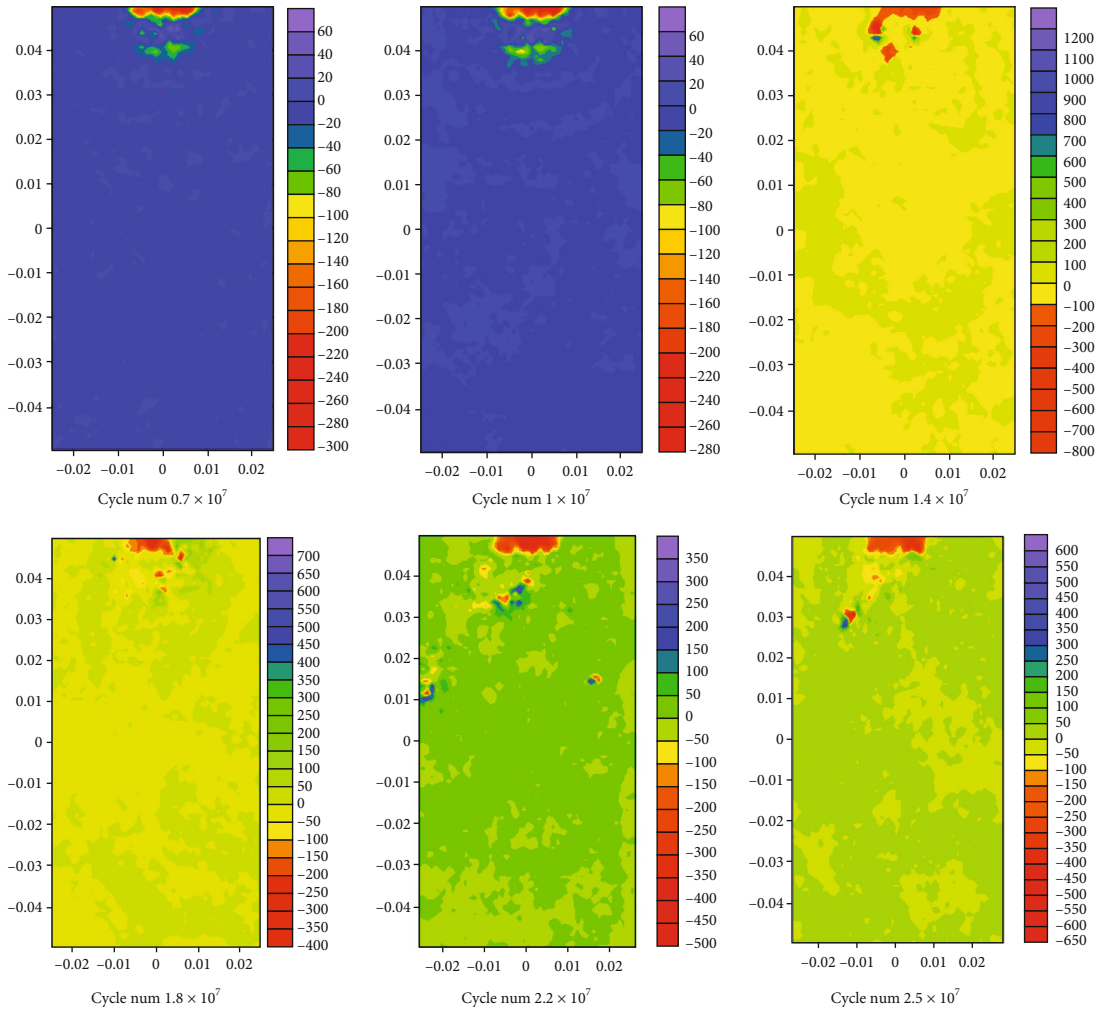

Figure 16: Distribution of stress field in rock under ultrasonic vibration excitation.

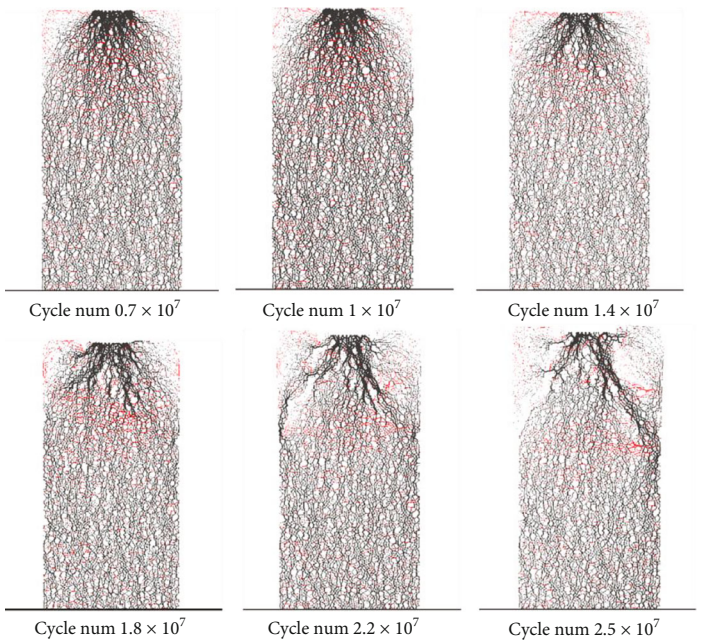

Figure 17: Distribution of force chain in rock under ultrasonic vibration excitation.

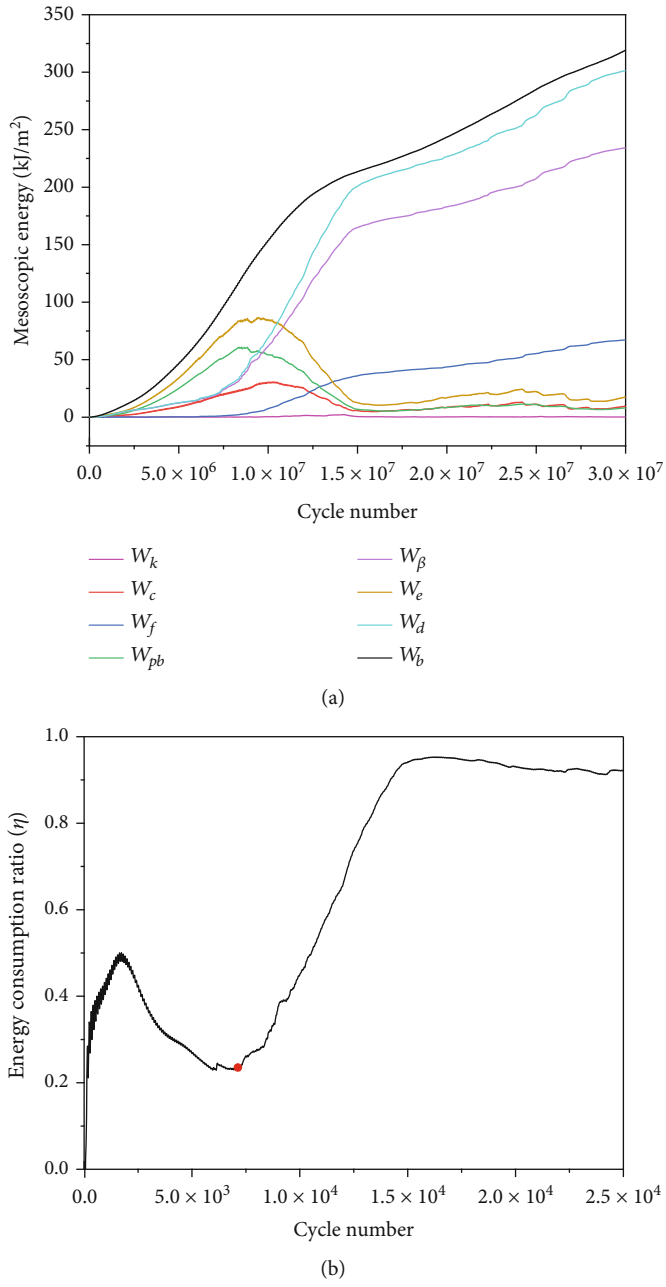

Figure 18: Energy evolution in rock breaking stimulated by ultrasonic vibration. (a) Energy evolution curve. (b) Energy dissipation coefficient evolution curve.

The energy dissipation coefficient is defined as:

$$\eta = \frac{W_\beta}{W_b}. \tag{13}$$

The energy dissipation coefficient curve reflects the change of energy utilization rate in the process of rock fracture. As shown in Figure 18(b), at the initial stage of vibration excitation, the energy dissipation ratio increases rapidly. In this process, the elastic deformation of the rock continuously occurs under the vibration load, and the input energy is partially converted into the strain energy of the sample, and the rest energy is dissipated in the form of friction energy generated by particle friction. When the dissipation coefficient reaches 50% of the peak value, this coefficient begins to decline until the rock failure occurs. This is because the proportion of dissipated energy decreases with the significant increase of strain energy; subsequently, with the rapid release of strain energy and the cumulative expansion of mesocracks, the energy dissipation coefficient curve rises again until the rock is completely destroyed and the curve tends to be stable.

Figure 19 compares the evolution curves of the energy dissipation coefficient under four static loads. In the initial stage, the four curves basically coincide, indicating that the

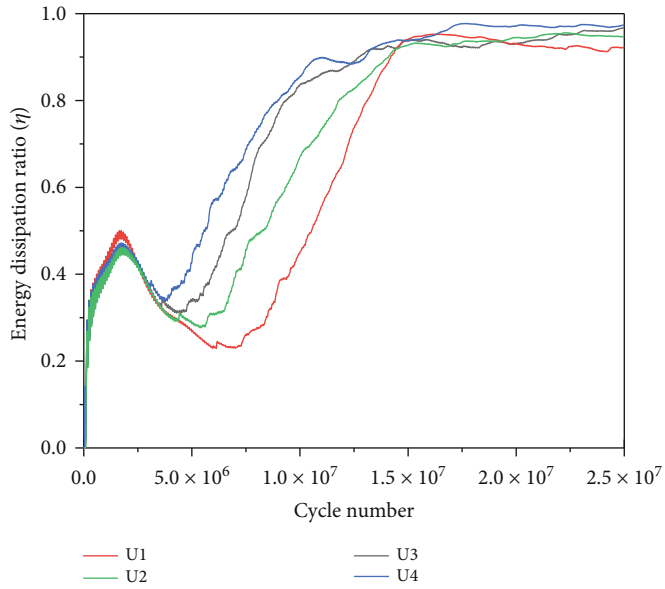

Figure 19: Evolution of energy consumption coefficient under different static load.

static load has little effect on strain energy and friction energy. With the increase of static load, the failure time of the rock sample is advanced and the energy dissipation ratio at failure also increases. It suggests that static load promotes plastic deformation in the rock sample and accelerates the speed of rock damage and fracture.

6. Conclusions

In this study, the laboratory test and discrete element simulation test of rock fracture under the excitation of ultrasonic vibration were conducted, and the failure characteristics and damage mechanism of brittle red sandstone under the excitation of ultrasonic vibration were analyzed from the macro- and mesoperspectives. The conclusions are drawn as follows:

(1) According to the strain curve obtained from the test, the deformation process of the rock sample can be divided into three stages, compaction stage, elastic deformation stage, and damage stage. Under the excitation of ultrasonic vibration, the rock has the maximum intrusion depth; after reaching this depth, the macrocracks are quickly penetrated, and the rock failure can be caused. The static load accelerates the failure rate of the rock mass, and has a good exponential relationship with the maximum intrusion depth and the maximum failure depth of rock

(2) The particle flow software PFC2D is used to simulate rock fracture under the excitation of ultrasonic vibration, and the simulated failure mode of the rock sample is completely consistent with the test results. Based on the simulated rock fracture distribution, the failure mechanism of rock under the excitation of ultrasonic vibration is revealed. Specifically, shear failure first occurs at the point of maximum shear stress of the rock sample, and the stress concentration makes the edge area of the excitation surface crack and expand towards the maximum shear stress direction; an X-shaped macrofracture zone is gradually formed inside the rock and develops to the free surface at both ends, and rock failure is caused finally

(3) The simulation results of the stress field and displacement field show that the obvious layering effect of the internal displacement field of rock under the excitation of ultrasonic vibration is significant, and the particle bond of particles in rock at the junction of high and low displacement fields is more likely to fracture and produce microcracks. There are high-stress and strong chain concentration areas in the area of excitation surface, and the intersection of compressive stress and tensile stress occurs at the fracture of the rock mass

(4) In the process of ultrasonic vibration excitation, the input energy is mainly dissipated in the generation of new cracks and the staggered friction between particles. The static load can effectively improve the utilization rate of rock fracture energy, and then shorten the failure time of the rock mass

Data Availability

The data that support the findings of this study are available from the corresponding author upon reasonable request.

Conflicts of Interest

The authors declare that they have no conflicts of interest.

Acknowledgments

This research was supported by the National Natural Science Foundation of China (No. 51874282), the Six Talent Peaks Project in Jiangsu Province (No. GDZB-052), and the Key Research and Development Projects of China Pingmei Shenma Group. The authors are grateful for these supports.

References

[1] S. Sherrit, X. Bao, Z. Chang, B. P. Dolgin, Y. Bar-Cohen, and D. Pal, "Modeling of the ultrasonic/sonic driller/corer: USDC," in *2000 IEEE Ultrasonics Symposium. Proceedings. An International Symposium (Cat. No.00CH37121)*, vol. 1, pp. 691–694, San Juan, PR, USA, 2000.

[2] M. Tomizuka, M. Badescu, S. Sherrit, X. Bao, Y. Bar-Cohen, and B. Chen, "*Auto-Gopher: a wire-line rotary-hammer ultrasonic drill*," in *Sensors and Smart Structures Technologies for Civil, Mechanical, and Aerospace Systems 2011*, pp. 1–8, San Diego, California, United States, 2011.

[3] M. Wiercigroch, J. Wojewoda, and A. M. Krivtsov, "Dynamics of ultrasonic percussive drilling of hard rocks," *Journal of Sound and Vibration*, vol. 280, no. 3-5, pp. 739–757, 2005.

[4] D. Zhao and S. Sangesland, *Dynamical Analysis of Drill Bit with Ultrasonic Vibration*, OMAE, 2015.

[5] N. Li, W. Chen, P. Zhang, and G. Swoboda, "The mechanical properties and a fatigue-damage model for jointed rock masses subjected to dynamic cyclical loading," *International Journal of Rock Mechanics and Mining Sciences*, vol. 38, 2001.

[6] M. N. Bagde and V. Petros, "Fatigue properties of intact sandstone samples subjected to dynamic uniaxial cyclical loading," *International Journal of Rock Mechanics and Mining Sciences*, vol. 42, no. 2, pp. 237–250, 2005.

[7] L. Yang, Y. Jiang, S. Li, and B. Li, "Experimental and numerical research on 3D crack growth in rocklike material subjected to uniaxial tension," *Journal of Geotechnical and Geoenvironmental Engineering*, vol. 139, no. 10, pp. 1781–1788, 2013.

[8] Y. Li, S. Zhang, and X. Zhang, "Classification and fractal characteristics of coal rock fragments under uniaxial cyclic loading conditions," *Arabian Journal of Geosciences*, vol. 11, no. 9, 2018.

[9] E. Liu and S. He, "Effects of cyclic dynamic loading on the mechanical properties of intact rock samples under confining pressure conditions," *Engineering Geology*, vol. 125, pp. 81–91, 2012.

[10] W. Li, T. Yan, S. Li, and X. Zhang, "Rock fragmentation mechanisms and an experimental study of drilling tools during high-frequency harmonic vibration," *Petroleum Science*, vol. 10, no. 2, pp. 205–211, 2013.

[11] S. Li, S. Tian, W. Li, T. Yan, and F. Bi, "Research on the resonance characteristics of rock under harmonic excitation," *Shock and Vibration*, vol. 2019, Article ID 6326510, 11 pages, 2019.

[12] S. Yin, D. Zhao, and G. Zhai, "Investigation into the characteristics of rock damage caused by ultrasonic vibration," *International Journal of Rock Mechanics and Mining Sciences*, vol. 84, pp. 159–164, 2016.

[13] Y. Zhou, Q. Tang, S. Zhang, and D. Zhao, "The mechanical properties of granite under ultrasonic vibration," *Advances in Civil Engineering*, vol. 2019, Article ID 9649165, 11 pages, 2019.

[14] D. Zhao, S. Zhang, and M. Wang, "Microcrack growth properties of granite under ultrasonic high-frequency excitation," *Advances in Civil Engineering*, vol. 2019, Article ID 3069029, 11 pages, 2019.

[15] L. Zhang, X. Wang, J. Wang, and Z. Yang, "Mechanical characteristics and pore evolution of red sandstone under ultrasonic high-frequency vibration excitation," *AIP Advances*, vol. 11, no. 5, 2021.

[16] Z. T. Bieniawski and M. J. Bernede, "Suggested methods for determining the uniaxial compressive strength and deformability of rock materials," *International Journal of Rock Mechanics & Mining Sciences & Geomechanics Abstracts*, vol. 16, no. 2, pp. 138–140, 1979.

[17] Y. Zhou, D. Zhao, Q. Tang, and M. Wang, "Experimental and numerical investigation of the fatigue behaviour and crack evolution mechanism of granite under ultra-high-frequency loading," *Royal Society Open Science*, vol. 7, no. 4, 2020.

[18] J. Liu, H. Xie, J. Xu, and J. Pei, "Discussion on deformation and damping parameters of rock under cyclic loading," *Chinese Journal of Rock Mechanics and Engineering*, vol. 31, no. 4, pp. 770–777, 2012.

[19] J. A. Vallejos, J. M. Salinas, A. Delonca, and D. Mas Ivars, "Calibration and verification of two bonded-particle models for simulation of intact rock behavior," *International Journal of Geomechanics*, vol. 17, no. 4, 2017.

[20] S.-Q. Yang, W.-L. Tian, Y.-H. Huang, P. G. Ranjith, and Y. Ju, "An experimental and numerical study on cracking behavior of brittle sandstone containing two non-coplanar fissures under uniaxial compression," *Rock Mechanics and Rock Engineering*, vol. 49, no. 4, pp. 1497–1515, 2015.

[21] X. F. Li, H. B. Li, Y. Q. Liu, Q. C. Zhou, and X. Xia, "Numerical simulation of rock fragmentation mechanisms subject to wedge penetration for TBMs," *Tunnelling and Underground Space Technology*, vol. 53, pp. 96–108, 2016.

[22] K. Li, Y. Cheng, and X. Fan, "Roles of model size and particle size distribution on macro-mechanical properties of Lac du Bonnet granite using flat-joint model," *Computers and Geotechnics*, vol. 103, pp. 43–60, 2018.

[23] L. Ma, Z. Xu, K. Zheng, J. Yan, and S. Yang, "Vibration characteristics of aluminum surface subjected to ultrasonic waves and their effect on wetting behavior of solder droplets," *Ultrasonics*, vol. 54, no. 3, pp. 929–937, 2014.

[24] X. Wang, L. Guo, Z. Xu et al., "A new index of energy dissipation considering time factor under the impact loads," *Materials (Basel)*, vol. 15, no. 4, 2022.

[25] H. P. Xie, J. U. Yang, and L. I. Li-Yun, "Criteria for strength and structural failure of rocks based on energy dissipation and energy release principles," *Chinese Journal of Rock Mechanics and Engineering*, vol. 24, no. 17, pp. 3003–3010, 2005.

[26] X. Li, C. Li, W. Cao, and M. Tao, "Dynamic stress concentration and energy evolution of deep-buried tunnels under blasting loads," *International Journal of Rock Mechanics and Mining Sciences*, vol. 104, pp. 131–146, 2018.

[27] G.-L. Wang, T. C. Cao, F. Sun, X. X. Wen, and L. Zhang, "Study on the meso-energy damage evolution mechanism of single-joint sandstone under uniaxial and biaxial compression," *Advances in Materials Science and Engineering*, vol. 2021, Article ID 5245402, 27 pages, 2021.

[28] D. Meng, C. Zhu, X. Zhao, and S. Zhao, "Applying low-frequency vibration for the experimental investigation of clutch hub forming," *Materials (Basel)*, vol. 11, no. 6, 2018.

[29] Z. Jiang, H. Deng, T. Liu, G. Tian, and L. Tang, "Study on microstructural evolution of marble under cyclic dynamic impact based on NMR," *Ieee Access*, vol. 7, pp. 13043–13055, 2019.